RSC Advances

PAPER

View Article Online
View Journal | View Issue

Cite this: *RSC Adv.*, 2018, **8**, 10914

Enhanced photoreduction degradation of polybromodiphenyl ethers with Fe_3O_4-g-C_3N_4 under visible light irradiation†

Ying-Ying Shao,[a] Wei-Dong Ye,[a] Chun-Yan Sun,*[a] Chun-Lin Liu,[a] Qi Wang,[b] Chun-cheng Chen,[c] Jia-Yun Gu[a] and Xiao-Qing Chen[a]

Received 12th February 2018
Accepted 9th March 2018

DOI: 10.1039/c8ra01356j

rsc.li/rsc-advances

As typical persistent organic pollutants, polybrominated diphenyl ethers (PBDEs) have aroused high environmental concern due to their toxicity and recalcitrant degradation. Herein, we report the enhanced photoreduction degradation of polybromodiphenyl ethers with Fe_3O_4-g-C_3N_4 under visible light irradiation (>420 nm). A series of high activity photocatalysts Fe_3O_4-g-C_3N_4 (named FeOCN-*x*) have been synthesized by an *in situ* growth method. The characterization of the prepared FeOCN-*x* nanocomposites has been examined by SEM, TEM, ultraviolet-visible diffuse reflectance spectroscopy, a vibrating sample magnetometer, X-ray diffraction, X-ray photoelectron spectroscopy and Brunauer–Emmer–Teller surface area analysis. FeOCN-*x* hybrids all exhibit good magnetic separation properties with the saturation magnetization at 300 K varying from 0.4 to 6.3 emu g^{-1}. Under visible light irradiation, FeOCN-*x* hybrids show enhanced photocatalytic activity for the debromination of PBDEs compared with g-C_3N_4. Among all the hybrids, FeOCN-4 with a 4 wt% Fe_3O_4 content gives the highest reaction rate, which is 6.7 times as high as that in pure g-C_3N_4. The FeOCN-*x* nanocomposites not only exhibit good photostability, but could also be easily recovered by magnetism. The results of the kinetic isotope effects (KIE) and the trapping agent experiments show that the rate determining step in the degradation reaction of PBDEs with FeOCN-*x* is the rate of electron accumulation in the conductive band. A possible photoreductive mechanism has been proposed. This study shows that the easily magnetically separable recycled photocatalyst FeOCN-*x*, with high visible light activity, could be an excellent candidate for dealing with halogen pollutants.

1. Introduction

Persistent organic pollutants (POPs) have aroused significant concerns because of global distribution and bioaccumulation in the environment.[1] As typical persistent pollutants, polybrominated diphenyl ethers (PBDEs) have attracted particular attention in this field due to their extensive use as flame retardants and their toxicity being transmitted along the food chain.[2] Owing to increasing usage, high hydrophobicity and persistence, PBDEs have been detected in sediments, marine organisms, food samples, and human mother's milk.[1] Thus, it is important to investigate an efficient method for decontamination of PBDEs.[3–5] It is well known that photocatalysis is an effective technology for the degradation of PBEDs.[3–6] In our previous studies,[3] PBDEs were rapidly degraded with TiO_2 under UV irradiation. However, only 5% of the solar spectra belongs to UV light. In order to effectively utilize solar energy, it is vital to realize photocatalytic degradation of PBDEs under visible light, which accounts for 50% of the solar spectra.

In recent years, carbon nitride (C_3N_4) has received wide attention in catalytic applications due to its excellent visible light activity with a wide band gap of 2.7 eV ($E_{CB} = -1.3$ V, $E_{VB} = 1.4$ V *vs.* NHE, pH = 7; E_{CB} is the conduction band potential, E_{VB} is the valence band potential).[7] Yue *et al.* reported that g-C_3N_4 could split water into hydrogen with an electron donor under visible light irradiation.[8] g-C_3N_4 also showed good performance in visible-light-driven photocatalytic degradation of organic dyes.[9] Nevertheless, the low quantum efficiency of pure g-C_3N_4 needs to be improved in practical applications. Synthesis of the heterojunction photocatalyst is a feasible way to enhance the quantum efficiency of the photocatalyst.[10,11] As heterojunction materials with proper band gaps not only superpose the light response of composed semiconductors, but also help transform the photogenerated holes and electrons, this results in the enhanced photocatalytic capability.[12]

---

[a] Department of Chemistry, Shaoxing University, Shaoxing 312000, Zhejiang, PR China. E-mail: sunchunyan@usx.edu.cn

[b] School of Environment Sciences and Engineering, Zhejiang Gongshang University, Hangzhou, PR China

[c] Beijing National Laboratory for Molecular Sciences, Key Laboratory of Photochemistry, Institute of Chemistry, Chinese Academy of Sciences, Beijing 100190, PR China

† Electronic supplementary information (ESI) available. See DOI: 10.1039/c8ra01356j

On the other hand, the highly dispersive nature of g-C_3N_4 based-photocatalysts seriously hampers the use of recycled photocatalysts in applications.[13] The good dispersive properties of photocatalysts may cause a lot of loss in the process of recovery. Thus, the synthesis of a g-C_3N_4 based-heterojunction photocatalysts with an easily separated recycling property is required. Fe_3O_4 nanoparticles have attracted particular interest for the treatment of pollutants due to their high conductivity and matched energy band, but also their special magnetic separation properties for use in recycling.[14–17] Fe_3O_4-based heterojunction catalysts, such as Fe_3O_4/WO_3[16] and Fe_3O_4/graphene[17] both show easy separation recovery and improved visible light activity for degradation of contaminants. Fe_3O_4 has an energy band ($E_{CB} = 1.0$ V *vs.* NHE, pH = 7) that is matched with g-C_3N_4.[16] Therefore, the construction of a Fe_3O_4-g-C_3N_4 heterojunction should be a good strategy for both enhancing the visible light catalytic activity and for easy separation recycling.[18–22] For example, Ye *et al.*[18] reported that Fe_3O_4-g-C_3N_4 showed an improved efficiency for degradation of dyes under visible light irradiation and easy recycling use. Chi *et al.*[19] found that Fe_3O_4-g-C_3N_4 had a high photocatalytic activity performance for the oxidization of As(III) to As(V) and could be easily recovered by magnetism. Compared with the extensive research on the photocatalytic oxidation ability of Fe_3O_4-g-C_3N_4, the photocatalytic reduction performance of Fe_3O_4-g-C_3N_4,[22] especially on degradation of the halogen organic pollutants is quite rare, which may reveal another important application for Fe_3O_4-g-C_3N_4. Considering that PBDEs usually undergo reduction with a photocatalyst,[3] we propose that Fe_3O_4-g-C_3N_4 might perform a highly enhanced reduction of PBDEs compared with g-C_3N_4 under visible light and excellent recovery use performance in application.

In this work, we prepared a series of heterojunction catalysts Fe_3O_4-g-C_3N_4 (named FeOCN-*x*) with a simple *in situ* growth method. Decabromodiphenyl ether (BDE209) (Fig. S1†) a typical persistent organic pollutant was selected as the target substrate. The photocatalytic reduction abilities of FeOCN-*x* hybrids for degradation of BDE209 were investigated under visible light irradiation. The kinetic isotope effects (KIE) and trapping agent experiments were performed to further indicate the rate determining step of the photoreductive reaction and the reaction mechanism. To the best of our knowledge, this is the first report on the photoreduction degradation of halogen organic pollutants with magnetically separable Fe_3O_4-g-C_3N_4 under visible light irradiation.

2. Materials and methods

2.1 Materials

BDE209, humic acid and the total deuterium with methanol (CD_3OD) were purchased from Sigma-Aldrich (USA). Melamine, $FeCl_3 \cdot 6H_2O$, $FeCl_2 \cdot 4H_2O$, and $NH_3 \cdot H_2O$ solution (25%), were purchased from Chemical Co., Shanghai. 2-Propanol (i-PrOH), THF, DMF, DMSO, CH_3OH, C_2H_5OH, hexane, toluene, and acetone were analytical reagents (Chemical Co., Shanghai) and were used without further purification. Deionized and doubly distilled water were used throughout the study.

2.2 Synthesis and characterization of photocatalysts

g-C_3N_4 was prepared by thermal polycondensation of dicyandiamide according to the reported procedure.[25] Fe_3O_4-g-C_3N_4 hybrids were prepared as follows:[19] 1.0 g of g-C_3N_4 powder was added to 250 mL of ethanol/water (1 : 2, v/v) solution by ultrasonic treatment for 5 h. A certain amount of $FeCl_3 \cdot 6H_2O$ and $FeCl_2 \cdot 4H_2O$ were dissolved in the deionized water and then added to the g-C_3N_4 suspension. Aqueous ammonia was added to the mixture under stirring at 80 °C. The sample was rinsed with deionized water and dried at 80 °C. To elucidate the role of g-C_3N_4 and Fe_3O_4 on the photocatalytic activity, samples with different amounts of Fe_3O_4 in the hybrids were prepared. By adjusting the mass percentage ratio of Fe_3O_4 to g-C_3N_4, different amounts of Fe_3O_4 loaded g-C_3N_4, denoted as s FeOCN-*x*, (*x* = 2, 4, 6, 8, 10; *x* refers to the ratio of Fe_3O_4 to FeOCN-*x* wt%) were prepared. Pure g-C_3N_4 and Fe_3O_4 were synthesized for comparison.

The morphology of the catalyst samples were carried out by SEM (Hitachi S4300) and TEM (Philips CM200 FEG TEM at 200 kV). The XRD patterns were measured on a Regaku D/Max-2500 diffractometer with a Cu-Kα radiation source (1.5406 Å). UV-Vis absorption spectra were obtained with 10 × 10 mm quartz cuvettes by a Hitachi U-3010 spectrophotometer (Hitachi Co. Japan). The XPS spectra were performed using an ESCA lab 220i-XL spectrometer with an Al-Kα (1486.6 eV) X-ray source and a charge neutralizer. N_2 adsorption–desorption isotherms were obtained using a Quantachrome Autosorb-IQ instrument at 77 K. The specific surface areas were detected by the Brunauer–Emmer–Teller (BET) method. The magnetization curves were detected at room temperature with a varying magnetic field from −30 000 to 30 000 Oe on a BHV-55 vibrating sample magnetometer (VSM).

2.3 BDE209 dehalogenation experiments

BDE209 stock solution (1×10^{-3} mol L^{-1}) in tetrahydrofuran was diluted with methanol (1×10^{-5} mol L^{-1}). 10 mg FeOCN-*x* was added to 10 mL BDE209 solution in a Pyrex vessel. In order to reach the adsorption equilibrium, the suspension was stirred for 30 min in the dark before irradiation. The reaction solution was magnetically stirred during the irradiation. The Pyrex vessel was purged with N_2 for 15 min to remove O_2 and protected under a N_2 atmosphere during the irradiation. A PLS-SXE300 Xe lamp (Beijing Trusttech Co. Ltd.) was used as the light source. A cutoff filter ($\lambda > 420$ nm) was placed to ensure visible light irradiation. The degradation kinetics of BDE209 with catalysts were all assumed to fit with pseudo-first order. The experiments were repeated in triplicate. In the HA control experiment, a stock solution of HA was added to the reaction solution and the final concentration of HA was 5 mg L^{-1}. To investigate the effect of organic solvents on the reaction kinetics, a given amount of ethanol and methanol were added into BDE209 under identical conditions, the BDE209 stock solution (1×10^{-3} mol L^{-1}) in tetrahydrofuran was diluted with seven different organic solvents, respectively and isopropyl alcohol (0.33 mol L^{-1}) was added as a hole scavenger. To investigate the effect of holes scavenger on the reaction kinetics, a given amount of ethanol and methanol were added into BDE209 under identical conditions. The KIE experiment was performed in the CD_3OD with the same conditions as in CH_3OH.

In the degradation reaction, at given time intervals, 1.5 mL of suspension was sampled and centrifuged to separate the catalyst. The supernatant was filtered through a 0.22 μm membrane to remove the catalyst particles. The filtrates were used for HPLC analysis. BDE209 was quantified by HPLC. The HPLC was a SHIMADZU HPLC system (LC-20AT pump and UV/VIS SPD-20A detector) with a DIKMA Platisil ODS C-18 column (250 × 4.6 mm, 5 μm film thickness). The mobile phase was 2% H_2O in acetonitrile with 1 mL min^{-1} and the detector wavelength was at 240 nm. The quantification of BDE209 was obtained by a calibration curve with a BDE-209 standard solution. The degradation kinetics of BDE209 with catalysts were all assumed to fit with pseudo-first order.

In all cases, the degradation of BDE209 was assumed to be pseudo-first order kinetics, and the rate constant (k) was calculated by the following equation:

$$\ln(C_0/C) = kt \tag{1}$$

where C_0 was the initial concentration of BDE209, C is the concentration of BDE209 at time (t), and k was the pseudo-first order rate constant.

3. Results and discussion

3.1 Characterization of photocatalysts

As shown in Fig. 1 and S2,† the morphology and microstructure of g-C_3N_4, Fe_3O_4 and FeOCN-4 are characterized by SEM and TEM. The SEM image of C_3N_4 shows a sheet like structure, which has slightly irregular edges (Fig. S2†). After combining with Fe_3O_4, the sample of FeOCN-4 exhibits a roundish lamellar structure (Fig. S2†). The TEM images of g-C_3N_4 show the layered planar structure (Fig. 1a). Fig. 1b shows that the Fe_3O_4 samples are small nanoparticles with sizes range of 10–20 nm. As seen from Fig. 1c, the Fe_3O_4 nanoparticles disperse on the surface of C_3N_4 and firmly connect with the surface of the lamellar C_3N_4 to form a heterojunction interface, which contributes to the better transfer of photoelectrons and separation of charge carriers between Fe_3O_4 and C_3N_4.

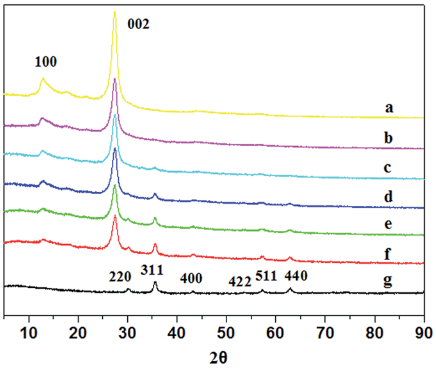

Fig. 2 XRD patterns of (a) pure g-C_3N_4, (b) FeOCN-2, (c) FeOCN-4, (d) FeOCN-6, (e) FeOCN-8, (f) FeOCN-10, (g) pure Fe_3O_4.

Fig. 2 shows the X-ray diffraction patterns of g-C_3N_4, Fe_3O_4 and FeOCN-x. The peak (100) at 12.75 corresponds to the in-plane structural packing motif. The strong peak at 27.28, indexed as (002), is related to the interlayer stacking peak of the aromatic system.[20] The XRD of Fe_3O_4 exhibits six diffraction peaks indexed as (220), (311), (400), (422), (511) and (440).[19,23] All of the hybrids of FeOCN-x show the characteristic peak of g-C_3N_4 and Fe_3O_4. With increasing Fe_3O_4 content, the relative diffraction intensity of g-C_3N_4 gradually decreases following the diffraction intensity of Fe_3O_4 and increasing in the FeOCN-x samples.

The optical properties of the Fe_3O_4-g-C_3N_4 samples were investigated by UV-Vis diffuse reflectance spectra. As shown in Fig. 3, pure g-C_3N_4 shows the two obvious absorbances at 312 nm in the UV region and 403 nm in the visible light region. Fe_3O_4 shows a broad strong absorption in the region of 250–700 nm. When combined with C_3N_4, FeOCN-x shows an enhanced absorption in both the UV (312 nm) and visible light region (403 nm). More importantly, the new absorption bands appear in the wavelength region of 450–600 nm after Fe_3O_4 loading. The intensity of the new absorption bands in FeOCN-x becomes stronger according to the increase of Fe_3O_4 content from 2 to 10 wt%. This implies that FeOCN-x may have higher visible light activity than that of pure g-C_3N_4.

The oxidation state and surface chemical compositions of the FeOCN-x hybrids were demonstrated by XPS measurements. As shown in Fig. 4, the XPS spectrum of C 1s shows three peaks

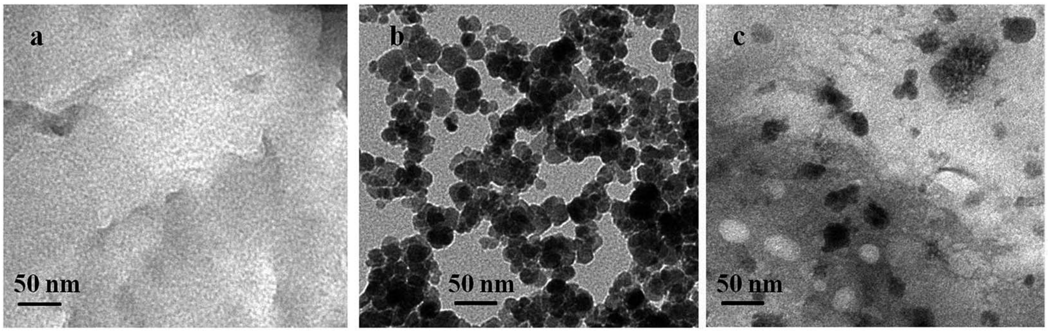

Fig. 1 TEM images of (a) pure g-C_3N_4; (b) pure Fe_3O_4; (c) FeOCN-4.

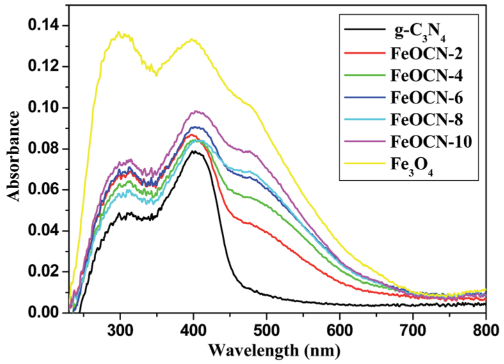

Fig. 3 UV-Vis-DRS of UV-Vis absorption spectra of pure g-C_3N_4, pure Fe_3O_4 and FeOCN-*x* (*x* = 2, 4, 6, 8, 10).

at 284.3 eV, 284.9 eV and 288.4 eV, due to the adventitious sp^2 carbon atoms bonded to N inside aromatic units and C–$(N)_3$ group. The XPS of N 1s has three peaks at 398.7 eV, 399.3 eV and 401.2 eV, corresponding to the sp^2 bonded N in the triazine rings, tertiary N in N–$(C)_3$ and N in amine group. The XPS of Fe 2p shows two signals at 710.4 eV and 724.1 eV indexed as Fe $2p_{3/2}$ and Fe $2p_{1/2}$, respectively.[20]

The magnetic properties of FeOCN-*x* samples have been investigated by magnetization curves between ±30 kOe at 300 K. As shown in Fig. 5, all of the FeOCN-*x* samples observe no hysteresis and the remanence and coercivity are close to zero. This demonstrates that FeOCN-*x* hybrids show typical superparamagnetic properties. The maximal saturation magnetization values of FeOCN-2, FeOCN-4, FeOCN-6, FeOCN-8, FeOCN-10 are 0.4, 0.7, 2.5, 4.7, 6.3 emu g^{-1}, respectively. Obviously, the saturation magnetization of FeOCN-*x* becomes stronger according to the increase in Fe_3O_4 content in the FeOCN-*x*. This indicates that the magnetic properties of FeOCN-*x* can be rationally controlled by adjusting the ratio of Fe_3O_4 to g-C_3N_4. The inset figure shows that the photocatalyst FeOCN-*x* can be easily separated by a permanent magnet.

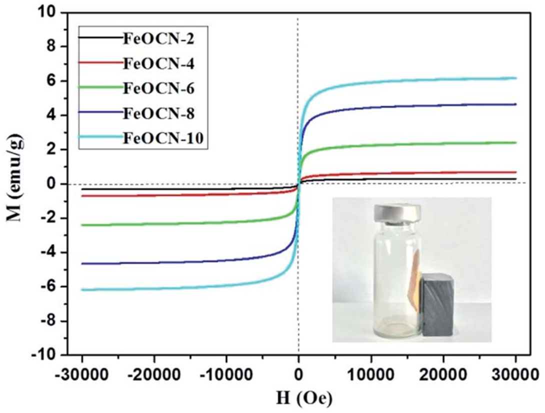

Fig. 5 Magnetization curves of FeOCN-*x* (*x* = 2, 4, 6, 8, 10).

3.2 Degradation of BDE209 with Fe_3O_4-g-C_3N_4 under visible light irradiation

As seen from Fig. 6, BDE209 itself shows little degradation under visible light irradiation. BDE209 also exhibits no degradation in the presence of Fe_3O_4 during the examination time. The degradation of BDE209 seldom occurs in a FeOCN-4/dark system. This means that the degradation of BDE209 with FeOCN-4 cannot occur without irradiation. In the presence of g-C_3N_4 under visible light irradiation, BDE209 shows slow degradation. Only 24% of BDE209 disappears after 1 h of irradiation. However, rapid degradation of BDE209 is observed with FeOCN-4 under visible light irradiation. More than 60% of BDE209 degrades after 1 h of irradiation. The kinetics were

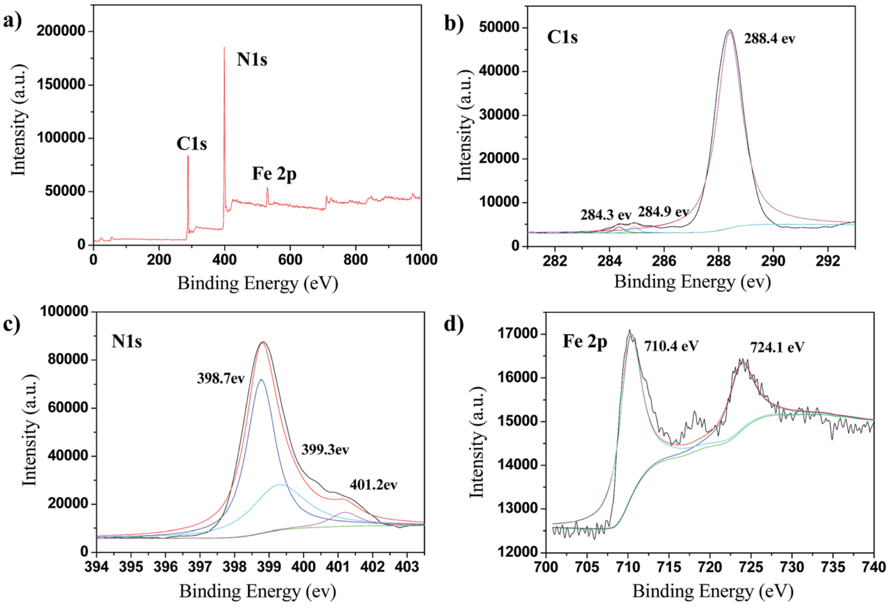

Fig. 4 XPS spectra of FeOCN-4. (a) Full-range spectrum; (b) C 1s; (c) N 1s; (d) Fe 2p.

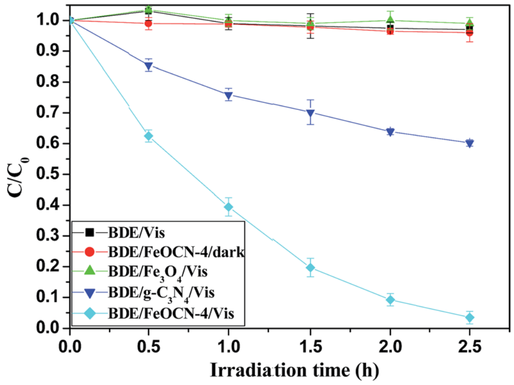

Fig. 6 Temporal curves of the degradation of BDE209 under different conditions. BDE209: 1.0 × 10^{-5} mol L^{-1}, FeOCN-4: 1 mg mL^{-1}, solvent: CH_3OH, wavelength > 420 nm, anoxic condition.

fitted to a pseudo-first-order process, giving a rate constant of $1.33 \pm 0.02\ h^{-1}$ ($t_{1/2} = 0.52$ h). Compared with g-C_3N_4 ($0.20 \pm 0.02\ h^{-1}$), the kinetic rate of reaction with FeOCN-4 has been improved 6.7 times. The product analysis by HPLC shows that BDE209 degrades to its lower brominated congeners in a stepwise way (Fig. S3†). This indicates that FeOCN-4 shows an improved photocatalytic activity compared with pure g-C_3N_4.

3.3 Effects of various parameters

3.3.1 Effects of photocatalyst. The photoreductive activity of FeOCN-*x* hybrids (*x* = 2, 4, 6, 8, 10) has been investigated by debromination of BDE209 under visible light irradiation. As shown in Fig. 7, all samples of FeOCN-*x* display an efficient degradation of BDE209. The degradation rates fit with a pseudo-first-order model kinetics. With the loaded mass percentage of Fe_3O_4 changing from 2 to 10 wt%, the photocatalytic activity of FeOCN-*x* first increases and then decreases. Among all of the hybrids, FeOCN-4 exhibits the best photoreductive activity for degradation of BDE209, which is about 6.7 times that of pure g-C_3N_4. The results may be attributed to the small amount of Fe_3O_4 forming at the heterojunction with g-C_3N_4, which can improve the separation of the photogenerated electron–hole pairs, and thus enhance the photoreduction activity of the photocatalysts. However, when a large amount of Fe_3O_4 is combined with g-C_3N_4, the Fe_3O_4 may act as the recombination centres of the photogenerated electrons and holes, covering the active sites on the g-C_3N_4 surface. This may lead to a reduction in the efficiency of the charge separation.

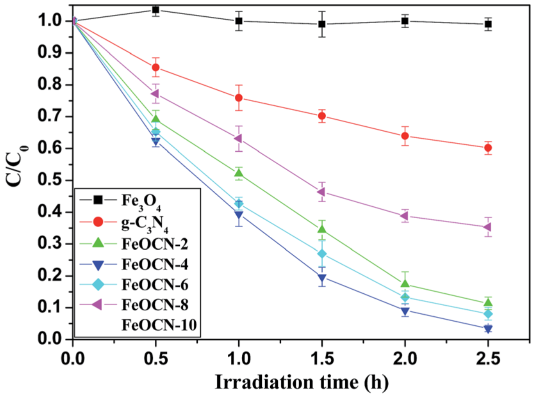

Fig. 7 Temporal curves of the photodegradation of BDE209 with FeOCN-*x* (*x* = 2, 4, 6, 8, 10) under visible irradiation. BDE209: 1.0 × 10^{-5} mol L^{-1}, FeOCN-*x*: 1 mg mL^{-1}, solvent: CH_3OH, wavelength > 420 nm, anoxic condition.

In order to reveal the nature of the effects of the photocatalyst, the pore structures of FeOCN-*x* have been examined by BET and BJH methods through N_2 adsorption at 77 K. The experimental results are shown in Table 1 and Fig. S4–S8.† As shown in Table 1, the specific surface area of g-C_3N_4 is only 7.51 $m^2\ g^{-1}$, but after Fe_3O_4 loading, the specific surface area of FeOCN-*x* largely improves from 7.51 to 28.54 $m^2\ g^{-1}$ (FeOCN-4). The difference in the loaded amount of Fe_3O_4 has little effect on the specific surface area of FeOCN-*x*, which changes from 20.21 to 28.54 $m^2\ g^{-1}$. The adsorption experiments were well matched to the value of the specific surface area of FeOCN-*x*. The adsorption isotherms of FeOCN-4 (Fig. S4†) shows that it is type IV according to the IUPAC classification with a mesopore structure.

3.3.2 Effects of organic solvents. In order to investigate the influencing factors on the photoreduction reaction, the debromination of BDE209 was carried out in seven organic solvents, respectively (Fig. 8). The degradation of BDE209 with FeOCN-4 was not observed in hexane or toluene solution, when the polarity of the organic solvent is weak. BDE209 is effectively degraded in the presence of FeOCN-4 in strong polarity solvents, such as tetrahydrofuran (THF), acetone, dimethyl sulfoxide (DMSO) *N*,*N*-dimethylformamide (DMF) and CH_3OH, under the same experimental conditions. The experimental results show that BDE209 can be effectively degraded in the higher polarity organic solvents, but debromination of BDE209 scarcely occurs in organic solvents with weak polarity. This result implies that the organic solvents participate in the degradation reaction and that a strong polarity organic solvent may help the electron transfer in the process of debromination. However, the polarity is not the only factor that influences the debromination of BDE209 with FeOCN-4. Although DMSO has the strongest polarity among all the seven organic solvents, the highest reaction rate was observed in CH_3OH because CH_3OH not only acts as the solvent, but can also be a holes scavenger in the debromination of BDE209.

3.3.3 Photostability of the photocatalyst. The photostability is an important factor for a photocatalyst in practical applications. Therefore, the recycling experiments were performed to test the photostability of FeOCN-*x*. As shown in Fig. 9, the photocatalyst FeOCN-4 still shows a strong photoreductive activity for the degradation of BDE209 after four cycles. The degradation rate of BDE209 exhibits no obvious decrease, proving that FeOCN-*x* has a good photostability. This result indicates that FeOCN-*x* shows an excellent heterojunction photocatalytic activity. At the heterojunction Fe_3O_4-g-C_3N_4, the recombination of electrons and holes is greatly inhibited, and the separation of electrons and holes is obviously enhanced.

Table 1 Physicochemical and estimated pseudo-first-order kinetic constant (k) for the degradation of BDE209 with Fe_3O_4-g-C_3N_4

Catalyst	Mass percentage of Fe_3O_4 (%)	S_{BET} (m^2 g^{-1})	BJH pore volume (cm^3 g^{-1})	Pore diameter (nm)	Absorption amount (%)	Kinetic constant k (h^{-1})
Fe_3O_4	—	79.78	0.37	16.92	0.22	—
g-C_3N_4	—	7.51	0.07	34.12	0.16	0.20 ± 0.01
FeOCN-2	0.02	21.91	0.10	23.41	0.23	0.88 ± 0.02
FeOCN-4	0.04	28.54	0.14	15.56	0.25	1.33 ± 0.01
FeOCN-6	0.06	26.55	0.12	14.16	0.24	1.02 ± 0.02
FeOCN-8	0.08	20.53	0.15	29.20	0.22	0.43 ± 0.02
FeOCN-10	0.10	20.21	0.14	26.20	0.22	0.35 ± 0.03

3.4 The rate determining step in the photoreduction reaction

It is well known that KIE, which is the ratio of the rate constants with the different isotopic substitution reactants, may help us to understand the mechanisms of a reaction and indicate the rate-determining step in the degradation reaction.[24] In the debromination process, at first, BDE209 is reduced by obtaining an electron from FeOCN-4 to produce the $BDE209^{\bullet-}$ radical and a sequential abstracting hydrogen from the solvent. Therefore, the KIE experiments may reveal important information about the mechanism of degradation of BDE209 by FeOCN-4. We performed degradation experiments under the same conditions with CD_3OD as the solvent instead of CH_3OH. As illustrated in Fig. 10, the result shows that the degradation rate of BDE209 is not obviously varied by the deuterium substituted solvent CD_3OD. The KIE is 1.02 ± 0.01, which shows no obvious KIE in the reaction. The results demonstrate that abstracting hydrogen from solvent is not the rate determining step in the debromination of BDE209 with FeOCN-4. The effect of the holes scavenger experiments have been investigated to reveal the rate determining step in the reaction. The experimental results (Fig. 10) show that the reaction rates are in the order of CH_3OH > C_2H_5OH corresponding to the oxidation ability of alcohols with holes on the valence band (VB) *via* dehydrogenation. In the process of the photocatalytic reaction, under light irradiation, this results in the generation of a VB hole and a conduction band (CB) electron. When the VB holes are trapped by a holes scavenger,[26] the electrons will accumulate on the CB. Under the anaerobic photocatalytic conditions, the CB electrons are the reductive species that contribute to the reduction of BDE209. The oxidation ability of the holes scavenger will directly influence the accumulation of the electrons on the CB. This indicates the rate of electrons accumulation on the CB largely influences the photoreductive degradation of BDE209 with FeOCN-*x*. In addition, in the presence of HA, the reaction rate increases in CH_3OH solution because HA may react with the holes on the VB. The oxygen control experiment also shows that O_2 inhibits the degradation of BDE209. O_2 can quickly react with electrons on the CB. This result again proves that it is the CB electrons that make BDE209 reductively debrominate and that the rate of accumulation of CB electrons is the rate-determining step.

3.5 The mechanism of reaction

A series of magnetically separated hybrids of FeOCN-*x* show highly improved photocatalytic activity for the degradation of PBDEs compared with g-C_3N_4 under visible light irradiation. The enhanced photoreductive ability of FeOCN-*x* is caused by the following three conditions: (i) improved visible light absorption; (ii) larger specific surface area; (iii) better photoinduced charge separation and electron transformation.

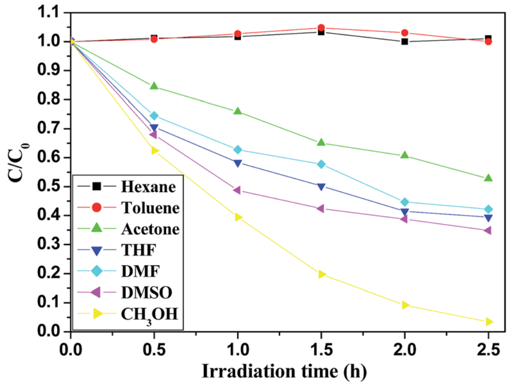

Fig. 8 Temporal curves of the degradation of BDE209 with FeOCN-4 in different solvents under visible light irradiation. BDE209: 1.0 × 10^{-5} mol L^{-1}, FeOCN-4: 1 mg/1 mL, wavelength > 420 nm, solvents: hexane, toluene, acetone, THF, DMF, DMSO, and CH_3OH, respectively; isopropyl alcohol, 0.33 mol L^{-1} (as hole scavenger); anoxic conditions.

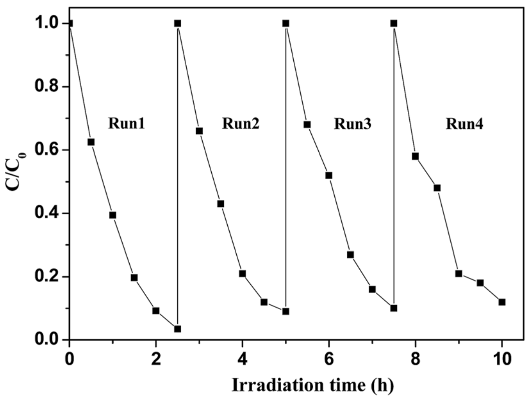

Fig. 9 Cycling runs in the degradation of BDE209 with FeOCN-4 under visible irradiation. BDE209: 1.0 × 10^{-5} mol L^{-1}, FeOCN-4: 1 mg mL^{-1}, solvent: CH_3OH, wavelength > 420 nm, anoxic conditions.

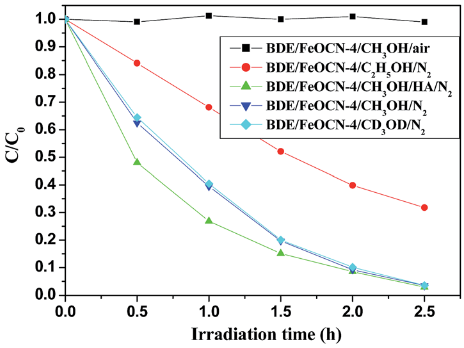

Fig. 10 The photoreductive degradation of BDE209 with FeOCN-4 under different conditions. BDE209: 1.0×10^{-5} mol L^{-1}, FeOCN-4: 1 mg/1 mL, wavelength > 420 nm.

Based on the above experiments, a possible reaction mechanism has been proposed for the degradation of PBDEs in CH_3OH solution by FeOCN-*x* (Fig. 11). Under visible light irradiation, the electrons are excited from the VB to the CB of g-C_3N_4. The valence band has a strong oxidation ability[26] and the electron on the CB has a reduction ability. PBDEs usually undergo reductive debromination. The CB electrons generated during the photocatalytic reaction might effectively reduce PBDEs to their lower bromo congeners under appropriate conditions.[3,6] In the Fe_3O_4-g-C_3N_4 system, due to the heterojunction between g-C_3N_4 and Fe_3O_4, and the CB edge potential of g-C_3N_4 (−1.30 eV)[7] is more negative than that of Fe_3O_4 (1.0 eV),[16] the photogenerated electrons in g-C_3N_4 could transfer to the CB of Fe_3O_4 *via* the interface. Due to the conductivity of Fe_3O_4. Being much higher than that of g-C_3N_4, the transport rate of the electrons is fast, which reduces the recombination of the photogenerated electrons and holes. The electrons in the CB of Fe_3O_4 could be further transferred to PBDEs. PBDEs receive the electrons on the CB of Fe_3O_4 and undergo reductive degradation. With an abstracting hydrogen atom from methanol (holes trapping agent), PBDES reduces to the debrominated products. Meanwhile, the photo-generated holes (h^+) in g-C_3N_4 can react with CH_3OH and cause the formation of inorganic small molecules, such as CO_2, H_2O, *etc.* Therefore, the efficient photoreduction of BDE209 can smoothly proceed. The Fe_3O_4 particles could act as electron traps to facilitate the separation of the photogenerated electron–hole pairs and promote the interfacial electron transfer process. FeOCN-4 shows the highest reaction rate among all of the FeOCN-*x* hybrids. This indicates that a small amount of Fe_3O_4 (mass percentage is 4 wt%) in FeOCN-*x* can largely improve the photoreductive activity.

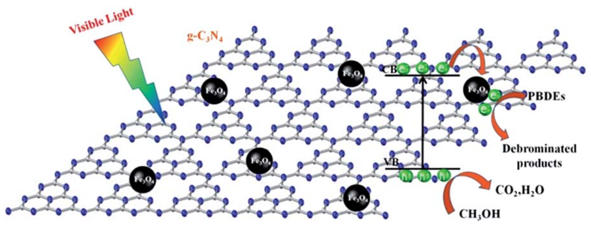

Fig. 11 Proposed mechanism of degradation of BDE209 with Fe_3O_4-g-C_3N_4 in CH_3OH solution under visible light irradiation.

4. Conclusions

The magnetically separated photocatalysts of FeOCN-*x* synthesized by a simple *in situ* growth method show highly enhanced photoreductive activity for degradation of BDE209 under visible light irradiation. FeOCN-*x* hybrids show the new absorption bands in the visible light region and a larger specific surface area compared with pure g-C_3N_4. Amongst the hybrids, FeOCN-4 with 4 wt% Fe_3O_4 content shows the highest reaction rate, with a rate up to 6.7 times as high as pure g-C_3N_4. More importantly, FeOCN-*x* not only shows good photostability for degradation of BDE209 after four runs experiments, but can also easily be separated by an external magnetic field. The KIE and trapping experiments indicate that the rate of electron accumulation in the CB is the rate determining step in the degradation reaction. This result shows that FeOCN-*x*, being a magnetically separable recycled photocatalyst with visible light activity, could be an excellent candidate for dealing with halogen organic pollutants.

Conflicts of interest

There are no conflicts to declare.

Acknowledgements

This research was generously supported by the National Science Foundation of China (No. 21107073 and 21477080).

References

1 C. A. de Wit, *Chemosphere*, 2002, **46**, 583–624.
2 B. Mai, S. Chen, X. Luo, L. Chen, Q. Yang, G. Sheng, P. Peng, J. Fu and E. Zeng, *Environ. Sci. Technol.*, 2005, **39**, 3521–3527.
3 C. Y. Sun, D. Zhao, C. C. Chen, W. H. Ma and J. C. Zhao, *Environ. Sci. Technol.*, 2009, **43**, 157–162.
4 A. Li, C. Tai, Z. S. Zhao, Y. W. Wang, Q. H. Zhang, G. B. Jiang and J. T. Hu, *Environ. Sci. Technol.*, 2007, **41**, 6841–6846.
5 R. J. Qu, C. G. Li, X. X. Pan, X. L. Zeng, J. Q. Liu, Q. G. Huang, J. F. Feng and Z. Y. Wang, *Water Res.*, 2017, **125**, 114–122.
6 C. Y. Sun, J. C. Zhao, H. W. Ji, W. H. Ma and C. C. Chen, *Chemosphere*, 2012, **89**, 420–425.
7 G. Liu, P. Niu, C. H. Sun, S. C. Smith, Z. G. Chen, G. Q. Lu and H. M. Cheng, *J. Am. Chem. Soc.*, 2010, **132**, 11642–11648.
8 B. Yue, Q. Y. Li, H. Iwai, T. Kako and J. H. Ye, *Sci. Technol. Adv. Mater.*, 2011, **12**, 7.
9 S. C. Yan, Z. S. Li and Z. G. Zou, *Langmuir*, 2010, **26**, 3894–3901.
10 Y. S. Chen, J. C. Crittenden and S. Hackney, *Environ. Sci. Technol.*, 2005, **39**, 1201–1208.
11 H. T. Yu, X. Quan and S. T. Chen, *J. Phys. Chem. C*, 2007, **111**, 12987–12991.

12 J. Yang, Z. H. Wen, X. X. Shen, J. Dai, Y. Li and Y. J. Li, *Chem. Eng. J.*, 2018, **334**, 907–920.

13 S. S. Zhao, S. Chen, H. T. Yu and X. Quan, *Sep. Purif. Technol.*, 2012, **99**, 50–54.

14 X. Yang, X. Zhang, Y. Ma, Y. Huang, Y. Wang and Y. J. Chen, *Mater. Chem.*, 2009, **19**, 2710–2714.

15 S. Xuan, W. Jiang, X. Gong, Y. Hu and Z. Chen, *J. Phys. Chem. C*, 2009, **113**, 553–558.

16 G. C. Xi, B. Yue, J. Y. Cao and J. H. Ye, *Chem.–Eur. J.*, 2011, **17**, 5145–5154.

17 L. Ren, S. Huang, W. Fan and T. Liu, *Appl. Surf. Sci.*, 2011, **258**, 1132–1138.

18 S. Ye, L. G. Qiu, Y. P. Yuan, Y. J. Zhu, J. Xia and J. F. Zhu, *J. Mater. Chem. A*, 2013, **1**, 3008–3015.

19 S. H. Chi, C. N. Ji, S. W. Sun, H. R. Jiang, J. Qu and C. M. Sun, *Ind. Eng. Chem. Res.*, 2016, **55**, 12060–12067.

20 S. Kumar, T. Surendar, B. Kumar, A. Baruah and V. Shanker, *J. Phys. Chem. C*, 2013, **117**, 26135–26143.

21 X. Zhou, B. Jin, R. Chen, F. Peng and Y. Fang, *Mater. Res. Bull.*, 2013, **48**, 1447–1452.

22 X. J. Bai, L. Wang, R. L. Zong and Y. F. Zhu, *J. Phys. Chem. C*, 2013, **117**, 9952–9961.

23 X. Y. Li, X. L. Huang, D. P. Liu, X. Wang, S. Y. Song, L. Zhou and H. J. Zhang, *J. Phys. Chem. C*, 2011, **115**, 21567–21573.

24 G. Parkin, *Acc. Chem. Res.*, 2009, **42**, 315–325.

25 G. Li, K. Gao, S. M. Wang, Q. Y. Xu, H. Wang, Z. Y. B. B. Huang, Y. Dai and J. Lu, *ACS Appl. Mater. Interfaces*, 2015, **7**, 9023–9030.

26 H. H. Ji, F. Chang, X. F. Hu, W. Qin and J. W. Shen, *Chem. Eng. J.*, 2013, **218**, 183–190.